Research Article

Biomimetic chitosan scaffolds with long-term controlled release of nerve growth factor repairs 20-mm-long sciatic nerve defects in rats

https://doi.org/10.4103/1673-5374.324860
Date of submission: February 26, 2021
Date of decision: May 21, 2021
Date of acceptance: July 19, 2021
Date of web publication: September 17, 2021

Fa-Dong Liu[1], Hong-Mei Duan[2], Fei Hao[1], Wen Zhao[2], Yu-Dan Gao[2], Peng Hao[2, *], Zhao-Yang Yang[2, 3, *], Xiao-Guang Li[1, 2, 3, *]

Graphical Abstract *The biomimetic NGF-chitosan scaffold (BCS) effectively promotes sciatic nerve regeneration and functional circuit reconstruction in rats*

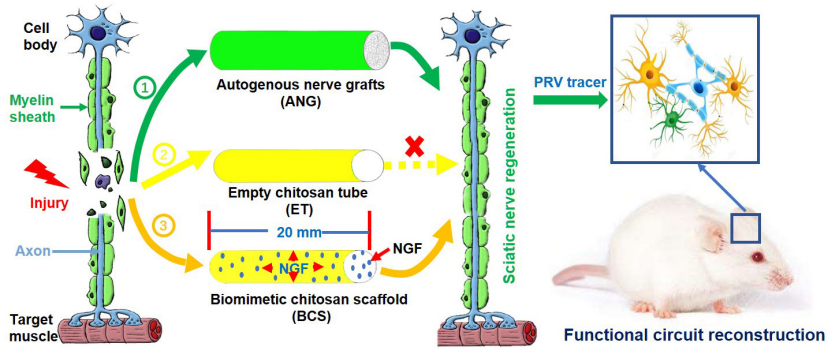

Abstract

Although autogenous nerve transplantation is the gold standard for treating peripheral nerve defects of considerable length, it still has some shortcomings, such as insufficient donors and secondary injury. Composite chitosan scaffolds loaded with controlled release of nerve growth factor can promote neuronal survival and axonal regeneration after short-segment sciatic nerve defects. However, the effects on extended nerve defects remain poorly understood. In this study, we used chitosan scaffolds loaded with nerve growth factor for 8 weeks to repair long-segment (20 mm) sciatic nerve defects in adult rats. The results showed that treatment markedly promoted the recovery of motor and sensory functions. The regenerated sciatic nerve not only reconnected with neurons but neural circuits with the central nervous system were also reconstructed. In addition, the regenerated sciatic nerve reconnected the motor endplate with the target muscle. Therefore, this novel biomimetic scaffold can promote the regeneration of extended sciatic nerve defects and reconstruct functional circuits. This provides a promising method for the clinical treatment of extended peripheral nerve injury. This study was approved by the Animal Ethics Committee of Capital Medical University, China (approval No. AEEI-2017-033) on March 21, 2017.

Key Words: axon; chitosan; functional recovery; myelin sheath; nerve growth factor; peripheral nerve injury; pseudorabies virus; regeneration; scaffold; sciatic nerve

Chinese Library Classification No. R445; R745; R318

Introduction

Although peripheral nerve injury remains prevalent after accidents, fortunately, short-distance peripheral nerve injuries can now be treated by surgery or tissue engineering scaffolds (Das and Srivastava, 2019; Wang et al., 2021; Zhang et al., 2021). However, for long (> 30 mm in humans, or > 10 mm in rats) peripheral nerve injury (Marquardt and Sakiyama-Elbert, 2013), direct surgical sutures are impossible because peripheral nerve elasticity is limited. At the same time, conventional scaffolds do not provide the necessary microenvironment for lengthy peripheral nerve regeneration. Thus, effectively bridging these kinds of peripheral nerve defects is difficult. At present, the gold standard for clinical treatment of extended peripheral nerve injury is still the autologous nerve graft (ANG) (Kornfeld et al., 2021). However, this procedure brings new trauma to the body region from which the graft is taken (Gu et al., 2011). In addition, the shapes of peripheral nerves in different parts of the body are very different, making sources limited (Rao et al., 2020).

Numerous studies have confirmed that composite scaffolds

[1]Beijing Key Laboratory for Biomaterials and Neural Regeneration, School of Biological Science and Medical Engineering, Beihang University, Beijing, China; [2]Department of Neurobiology, Capital Medical University, Beijing, China; [3]Beijing International Cooperation Bases for Science and Technology on Biomaterials and Neural Regeneration, Beijing Advanced Innovation Center for Biomedical Engineering, Beihang University, Beijing, China
*Correspondence to: Peng Hao, PhD, hp_sarah@126.com; Zhao-Yang Yang, PhD, wack_lily@163.com; Xiao-Guang Li, PhD, lxgchina@sina.com.
https://orcid.org/0000-0002-2968-1052 (Fa-Dong Liu); https://orcid.org/0000-0002-8509-8232 (Peng Hao)

Funding: *This study was supported by the National Natural Science Foundation of China, Nos. 31900749 (to PH), 31730030 (to XGL), 81941011 (to XGL), 31971279 (to ZYY), 31771053 (to HMD); and the Natural Science Foundation of Beijing of China, No. 7214301 (to FH).*
How to cite this article: *Liu FD, Duan HM, Hao F, Zhao W, Gao YD, Hao P, Yang ZY, Li XG (2022) Biomimetic chitosan scaffolds with long-term controlled release of nerve growth factor repairs 20-mm-long sciatic nerve defects in rats. Neural Regen Res 17(5):1146-1155.*

loaded with nerve growth factor (NGF) can promote the survival of neurons and accelerate axonal regeneration after sciatic nerve injury (Wang et al., 2012; Fu et al., 2013; Li et al., 2018; Mohamadi et al., 2018; Xia and Lv, 2018; Lackington et al., 2019). In rats, a chitosan-based nerve conduit loaded with NGF was capable of repairing 10-mm sciatic nerves and encouraging functional recovery that compared favorably with that of the autologous nerve grafts (Wang et al., 2012). However, the effectiveness of using chitosan scaffolds loaded with NGF for repairing longer distance (> 10 mm) nerve injury remains an open question. The objective of the present study was to determine whether a modified NGF-chitosan scaffold can repair 20-mm sciatic nerve gaps in adult rats.

Considering that hard chitosan scaffolds might cause compression and damage to surrounding tissue (Cao et al., 2018; Liu et al., 2021), we designed the elastic properties of natural sciatic nerves into an NGF-chitosan scaffold. Most time point-controlled release of NGF in previous studies had been less than 40 days (Kemp et al., 2011; Xu et al., 2011; Mohamadi et al., 2018), which might only be appropriate for short-distance (< 10 mm) peripheral nerve injury in rats. We recently showed that a stable regenerative microenvironment constructed with a biomimetic chitosan scaffold and long-term release of NGF (over a period of 8 weeks) would effectively promote the repair of 20-mm peripheral nerve injury. After 12 weeks, evaluation revealed that the sciatic nerve had successfully regenerated and that behavior had improved. In addition, functional reconstruction of neural circuits between regenerated peripheral nerves and the central nervous system were reported to facilitate the recovery of fine motion function and sensitive sensory function (Navarro et al., 2007). We studied the reconstruction of synaptic connections between regenerated sciatic nerves and the central nervous system using the cross-synaptic pseudorabies virus (PRV) tracing technique (Jia et al., 2019). We expected that the biomimetic NGF-chitosan scaffold (BCS) with control-released NGF would effectively promote nerve regeneration and functional recovery, so as to achieve the goal of replacing autogenous nerve transplantation and bring new hope for the repair of clinical nerve injuries.

Materials and Methods

Preparation of the BCS

In an improved method (Yang et al., 2015), under sterile conditions, a 2% (w/v) poly-N-acetyl glucosamine derived solution from 85% (w/v) deamidized chitosan (Sigma-Aldrich, St. Louis, MO, USA) in 100 mL of water containing 2% (w/v) acetic acid was plasticized by treatment with 1 g of lithium chloride. A 304 stainless steel mold (Newinvent, Wuxi, China) with a diameter of 1.8 mm and length of 20 cm was hung into the solution. The mold was rotated clockwise for five turns within 5 seconds, then the mold was removed vertically and placed diagonally into a 500-mL beaker (Shuniu, Chengdu, China). The beaker with the mold was placed in a 45°C oven and dried for 4–5 hours. This step was repeated nine times. NaOH (2 g) was then dissolved in 98 mL of pure water for preparing a 2% (w/v) NaOH solution, and the dried mold was soaked in a measuring cylinder containing the 2% (w/v) NaOH solution for 5–10 minutes. Deionized water was used to repeatedly clean the soaked NaOH mold, the outer chitosan tube was carefully removed from the mold, and the empty chitosan tube was cut to be 20 mm in length. The tube was soaked in 75% alcohol for 1 hour to dehydrate, and further soaked in anhydrous ethanol for 1 hour to fully dehydrate.

Under aseptic conditions, 10 mg chitosan particles (Sigma-Aldrich) were immersed in 10 mL deionized water at pH 7.2, centrifuged for 6 hours, and the supernatant was discarded. The expanded chitosan particles were frozen at –20°C for 24 hours and then frozen at 4°C for 10 hours. One-hundred nanograms NGF (Sigma-Aldrich) was then mixed with the above-mentioned chitosan particles in a 4°C solution. The dried chitosan particles loaded with NGF were added to a type-I collagen solution, vacuumed, and freeze-dried. The diameter of the chitosan particles was about 300 μm. Before surgery, a 10-mg chitosan carrier loaded with NGF (100 ng) was evenly injected into the inner wall of the chitosan scaffold and stored at 4°C for use.

Mechanical characteristics of the BCS and sciatic nerve

The stress-strain curves for the complete NGF-chitosan scaffold (n = 3) and sciatic nerve (n = 3) were measured in rats with a mechanical tensile tester (Instron5565, INSTRON, Boston, MA, USA). Three specific-pathogen-free (SPF) adult female Wistar rats, weighing 230–250 g, 10-week-old, were provided by the Charles River Laboratories (Wilmington, MA, USA). Rats were anaesthetized with an intraperitoneal injection of 3% sodium pentobarbital solution (30 mg/kg body weight; Sigma-Aldrich). The sciatic nerve was exposed and removed. The NGF-chitosan scaffold and sciatic nerve were cut into 25-mm samples to be tested. The sample was placed into the measuring clamp, the tension was slowly loaded at a rate of 1 mm/min. We paid attention to any deformation of the sample in the process of stretching, and stopped testing when the sample fractured. For the nanoindentation test (UMT-2, Bruker, Billerica, MA, USA), a total of 3 NGF-chitosan scaffolds were measured, and five sites for detecting nano-indentation were randomly selected from each scaffold for testing.

Kinetics of NGF release

According to the instructions of the NGF-enzyme linked immunosorbent assay (X-Y BIOTECHNOLOGY, Shanghai, China), a 96-well plate was set up with blank wells and sample wells to be tested, and 100 μL phosphate buffer saline solution was added to each well. Then, a 1-mg chitosan carrier (10 ng NGF) was added to the phosphate buffer saline solution one well at a time. The NGF-enzyme linked immunosorbent assay was used to determine the kinetics of NGF release at 1, 3, 6, 12 hours, 1, 3 days, and 1–10 weeks. Absorbance was read at 450 nm using an enzyme linked immunosorbent assay plate reader (Model 680, Bio-Rad, Hercules, CA, USA).

Animal and surgical procedures

The study was by the ethical standards of the Animal Ethics Committee of Capital Medical University (approval No. AEEI-2017-033) on March 21, 2017. All experiments were designed and reported according to the Animal Research: Reporting of *In Vivo* Experiments (ARRIVE) guidelines. One-hundred and three SPF adult female Wistar rats, weighing 230–250 g, 10-week-old, were provided by the Charles River Laboratories (Wilmington, MA, USA). Rats were randomly divided into five groups: sham control (SHAM), lesion (LC), empty tube (ET), ANG, and BCS groups.

Animals were anesthetized with an intraperitoneal injection of 3% sodium pentobarbital solution (30 mg/kg body weight). The sciatic nerve was exposed by making a skin incision and splitting the underlying muscles in the left lateral thigh. In the BCS group (n = 27), after excising 20 mm of the left sciatic nerve, the BCS was implanted into the 20-mm gap and stitched to the ends of the remaining sciatic nerve with single 10/0 stitches (Ethilon®, Ethicon Inc., New Brunswick, NH, USA). For rats in the ET group (n = 17), an ET was implanted into the 20-mm gap. For rats in the ANG group (n = 21), a 20-mm-long

segment of the left sciatic nerve was excised and not turned over, then immediately re-implanted with 10/0 stitches. For rats in the LC group (n = 17), 20 mm of the left sciatic nerve was excised, and rats received no treatment. For the SHAM group (n = 21), the left sciatic nerve was exposed but not injured in any way. Muscles and skin were closed in layers with 6/0 stitches. The skin of the operated area was disinfected with iodine. Rats were then intraperitoneally injected with 0.5 mL penicillin (1.0×10^4 U; North China Pharmaceutical Co., Shijiazhuang, China) to prevent infection after surgery. The experimental rats were kept on a 12-hour light/dark cycle in a room at 24–26°C and a relative humidity of 35–45%. After surgery, all animals were housed and fed routinely, and monitored for changes in their general conditions.

Morphological evaluation of the regenerative sciatic nerve

To observe the number of regenerated nerves in the NGF-chitosan scaffolds at acute time points, rats in the BCS group were sacrificed by intraperitoneal overdose of pentobarbital sodium solution (60 mg/kg body weight) at 7 and 10 days post-injury (n = 3 each day). The middle portion of the regenerated nerve tissue was cut into transverse sections on a cryostat microtome (CM1520, Leica, Frankfurt, Germany). Sections (four slices/rat) were immunostained with neurofilament-200 (NF200) antibody (chicken, 1:2000, Cat# AB5539, RRID: AB_11212161, Sigma-Aldrich) overnight at 4°C. The sections were then incubated in the secondary antibody (Alexa Fluor 488-conjugated goat anti-chicken IgY; 1:200, Cat# A11039, RRID: AB_2534096, Thermo Fisher) for 6 hours at room temperature. The sections were then observed with a confocal microscope (TCS SP8, Leica). All axons visible in the cross sectioned (600 μm × 600 μm) confocal image were counted using Image-Pro Plus 6.0 software (Media Cybernetics, Rockville, MD, USA).

Twelve weeks after surgery, eight rats from each group were sacrificed by intraperitoneal overdose of pentobarbital sodium solution (60 mg/kg body weight). The injured region were then observed. Then, the sciatic nerves in the center of the injury area (3 mm) were cut into transverse sections (n = 4) for immunofluorescence staining. The sections were washed three times (3 minutes each time) with 0.01 M phosphate buffer saline. The sections (four slices/rat) were incubated in the blocking solution (ZSGB-BIO, Beijing, China) for 1 hour at room temperature, followed by incubation with NF200 antibody (chicken, 1:2000, Cat# AB5539, RRID: AB_11212161, Sigma-Aldrich) and S100 antibody (rabbit, 1:100, Cat# ab52642, RRID: AB_882426, Abcam, Cambridge, UK) overnight at 4°C. The sections were then incubated in secondary antibodies for 6 hours at room temperature. The secondary antibodies were Alexa Fluor 594-conjugated goat anti-chicken IgY (1:200, Cat# A32759, RRID: AB_2762829, Thermo Fisher) and Alexa Fluor 488-conjugated goat anti-rabbit IgG (1:200, Cat# A32731, RRID: AB_2633280, Thermo Fisher). 4′,6-Diamidino-2-phenylindole (1:1000, Sigma) was used to stain the nuclei. The sections were observed with a confocal microscope (TCS SP8, Leica). A field of view was randomly selected for each section to observe axon morphology. The number of axons visible in the whole cross section (1.2 mm × 1.2 mm) were counted using Image-Pro Plus 6.0 software. The fiber count generated by the software has been manually verified.

In addition, the sciatic nerves from the SHAM, ANG, and BCS groups were cut into longitudinal sections (n = 4). As mentioned above, sections were then stained with NF200 antibody and a secondary antibody. The sections were photographed under appropriate microscope settings (BX-61, Olympus, Tokyo, Japan).

Morphological evaluation of the myelin sheath

Twelve weeks after surgery, four rats from each group were sacrificed by intraperitoneal overdose of pentobarbital sodium solution (60 mg/kg body weight). The sciatic nerves in the center of the injury area (3 mm) were cut into semi-thin sections. The sections were incubated with 1% toluidine blue dye (Solarbio, Beijing, China) for 10 minutes at room temperature, and observed under a microscope (BX-51, Olympus). The remaining nerve specimens were cut into ultra-thin sections with a thickness of 60 nm and stained with lead citrate and uranyl acetate. Stained sections were observed using a transmission electron microscope (HT7700, Hitachi, Tokyo, Japan).

PRV retrograde tracing

Twelve weeks after surgery, PRV retrograde tracing was performed. The titer of PRV-enhanced green fluorescent protein (BrainVTA (Wuhan) Co., Ltd., Wuhan, China) was 2.0×10^9 plaque forming units/mL. Eight rats in each group were anesthetized by intraperitoneal injection of 3% pentobarbital sodium (30 μg/g body weight). Then, 2 μL PRV was injected into the sciatic nerve, 5 mm away from the injured area. All injections were made with a 36 GA injection needle (World Precision Instruments, Sarasota, FL, USA) at a rate of 1 μL/min. The needle was held in place for an additional 30 seconds following the injection. Five days after PRV injection, the rats were over anesthetized (pentobarbital sodium solution, 60 mg/kg body weight) to death and perfused through the heart. The spinal cord, dorsal root ganglion (DRG), and brain were sectioned on a cryostat microtome (DMR, Leica). The DRG sections were incubated with calcitonin gene-related peptide (CGRP) antibody (goat, 1:400, Cat# ab36001, RRID: AB_725807, Abcam) at 4°C for 24 hours. The secondary antibody was Alexa Fluor 594-conjugated donkey anti-goat IgG (1:200, Cat# A32758, RRID: AB_2762828, Thermo Fisher). 4′,6-Diamidino-2-phenylindole was used to stain the nuclei. The sections (five slices/rat) were observed under a confocal microscope. The number of neurons at several locations was analyzed using Image-Pro Plus 6.0 software. PRV-positive motor neurons located in the left anterior horn of the spinal cord were counted. Neurons (CGRP/PRV double positive cells) in the entire DRG section (1.2 mm × 1.2 mm) were counted. PRV-positive neurons in the reticular nucleus, vestibular nucleus, and M1 region of motor cortex were counted separately in the sections.

Behavioral tests

For assessing nerve function, we used the sciatic nerve-function index (SFI). Five rats were selected from each group for testing at 2, 4, 6, 8, 10, and 12 weeks after surgery. Cardboard was used to make a 60 cm × 10 cm × 10 cm carton that was open at both ends. For each test, white paper was cut to the same length and width as the carton and laid at the bottom. After dipping the left hindfeet in red ink and the right hindfeet in blue ink, rats in each group were placed in the carton. Rats were placed at one end of the carton and then walked to the other end, leaving clear footprints on the white paper. The SFI was calculated using the following formula (Bain et al., 1989): SFI = –38.3 (EPL – NPL) / NPL + 109.5 (ETS – NTS) / NTS + 13.3 (EIT – NIT) / NIT – 8.8. The PL (print length) is the distance from the heel to the third toe, the TS (toe spread) is the distance from the first to the fifth toe, and the intermediary IT (toe spread) is the distance from the second to the fourth toe. EPL, ETS and EIT represent the records of the injured foot, while NPL, NTS and NIT represent the records of the non-operative foot. A value of negative 100 indicates total impairment.

For sensory recovery in rats, an Austerlitz pin (Entomoravia, Austerlitz, Czech) was used to evaluate high threshold mechanical sensitivity responsiveness of the Wistar rats, as has been previously described (Sakuma et al., 2016). After sciatic nerve injury, we gently pricked the surface of the affected hindfoot with the pin, without penetrating the skin or moving the claw. The outermost part of the plantar of the hind claw (the sensory area for the sciatic nerve) was divided into 5 areas. The needle test was performed from the outermost toe to the heel. When the animal significantly moved its claws, the response was considered positive. A value of 1 was assigned for the area, and then the next area was tested. If all pinpricks got a positive response, the total score was 5. After the surgery, five rats in each group received the pinprick assay each week.

Analysis of muscle atrophy

Twelve weeks after surgery, four rats from each group were sacrificed to determine the muscle wet-weight ratio between the injured and uninjured side. Both anterior tibial muscles were harvested and immediately weighed with an electronic balance (MP200-1, Mettler-Toledo, Zurich, Switzerland). The left tibialis anterior muscle was sectioned and stained with traditional hematoxylin-eosin (HE). In brief, the sections were put into hematoxylin dye (ZSGB-BIO) and incubated at room temperature for 10 minutes. The sections were washed with double distilled water to remove the dye and then placed in running tap water for 10 minutes. The sections were then placed in eosin solution (ZSGB-BIO) at room temperature for 30 seconds, dehydrated with gradient alcohol, made transparent with xylene, and sealed with neutral gum. The sections were photographed using a light microscope.

Analysis of motor endplate

Twelve weeks after surgery, the mid-belly of the tibialis anterior muscle (n = 5) was sliced longitudinally with a cryostat microtome. All sections were divided into 2 groups: group 1 for acetylcholinesterase (AChE) staining, and group 2 for immunohistochemical staining. Group 1 sections (five slices/rat) were incubated in AChE buffer (Baso, Zhuhai, China) for 2 hours. The sections were then dehydrated with gradient alcohol, made transparent with xylene, and sealed with neutral gum. The sections were then photographed using a light microscope. The integrated optical density (IOD) of the AChE in the image was calculated. Group 2 sections (five slices/rat) were stained with fluorescent Synapse1 (SYN) antibody (rabbit, 1:200, Cat# 2312S, RRID: AB_2200102, Millipore) and α-Bungarotoxin (BTX) (bungarus multicinctus, 1:500, Cat# B13423, RRID: AB_2891137, Molecular Probes). Immunofluorescence staining following the same procedure as the AChE staining. Images were captured using a confocal microscope. The mean area of the motor endplate and the IOD of AChE were measured using Image-Pro Plus 6.0 software.

Statistical analysis

All data are expressed as the mean ± standard deviation (SD) and were statistically analyzed using SPSS 16.0 software (SPSS, Inc., Chicago, IL, USA). Significance was determined by one-way analysis of variance followed by Fisher's least significant difference test. The Student's t-test was used to compare the two-sample means. Values were considered significantly different at $P < 0.05$.

Results

Characterization of the NGF-chitosan scaffold

The total length of the NGF-chitosan scaffold used for transplantation was 20 mm. The inner diameter of the NGF-chitosan scaffold was 1.8 mm, the outer diameter was 3.0 mm, and the thickness of the tube wall was 0.6 mm (**Figure 1A**).

After our modification, the BCS has similar physical properties to the rat sciatic nerve (**Figure 1B**). The maximum stress withstood by the BCS was 2.656 ± 0.214 MPa and the maximum stress withstood by sciatic nerve was 2.094 ± 0.185 MPa ($P < 0.05$, n = 3). The elastic modulus was 9.692 ± 0.122 MPa for the BCS and 9.644 ± 0.228 MPa in normal sciatic nerves. In addition, breaking-point elongation was 32.1 ± 4.2% for the BCS and 31.8 ± 6.5% for the sciatic nerves. There was no difference in elastic modulus (P = 0.689, n = 3) and breaking elongation (P = 0.946, n = 3) between the two groups. This biomimetic elastic design might avoid any abnormal sensation caused by the scaffold around the sciatic nerve. Nanoindentation testing the BCS (**Figure 1C**), showed that the hardness at maximum load was 0.123 ± 0.044 GPa, the modulus at maximum load was 1.068 ± 0.164 GPa, and the displacement at maximum load was 4244.5 ± 511 nm. This indicated that the micromechanical properties of chitosan scaffolds also could deform quite a bit.

NGF was released at a rate of 15.7 ± 2.08% within the first 1 hour (**Figure 1D**). At 12 hours, total NGF release reached 34.0 ± 5.57%. This facilitated rapid deployment of large amounts of NGF in the microenvironment to promote nerve regeneration. At the following time point, NGF release began to slow, and by the 8th week, the total sustained release rate of NGF had reached 96 ± 2.65%. No release of NGF was detected at weeks 9 or 10. This indicates that the chitosan carrier could release NGF stably for 8 weeks, showing its potential to provide long-term nutritional support for repair of lengthy peripheral nerve injury.

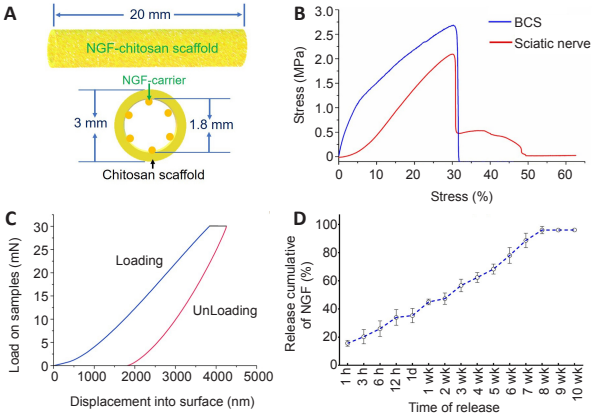

Figure 1 | **Characterization of the BCS.**
(A) Schematic diagram of the BCS. (B) The stress-strain curves for the BCS (n = 3) and the rat sciatic nerve (n = 3). (C) Nanoindentation tests of the BCS. (D) The profile of NGF release from the BCS *in vitro* for at least 8 weeks (n = 3). Data are expressed as mean ± SD. BCS: Biomimetic NGF-chitosan scaffold; NGF: nerve growth factor.

General observation of the regenerated sciatic nerve

Twelve weeks after surgery, the injured areas were observed in each group (**Figure 2A** and **B**). Macroscopic signs of neuroma formation, seroma, and inflammation were absent. In the SHAM group, the intact sciatic nerve was observed, while no significant sciatic nerve regeneration was observed in the LC group. No significant neural tissue regeneration was observed in the chitosan tube of the ET group. The nerve defect was successfully bridged by autologous nerve transplantation in the ANG group. The regenerated nerve tissue in the BCS group was able to bridge the 20-mm gap and showed normal peripheral nerve features. Thus, both BCS and ANG can be used to repair a 20-mm sciatic nerve defect in rats, but an empty tube alone failed to bridge the nerve defect (**Figure 2C**).

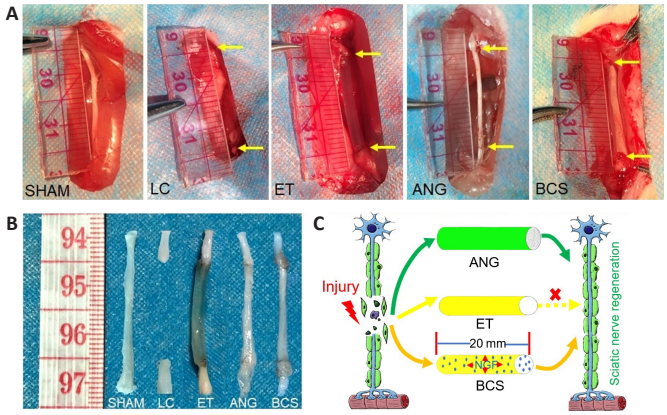

Figure 2 | General observation of the regenerated sciatic nerve 12 weeks after surgery.

(A) The left sciatic nerve was exposed to reveal a 20-mm regenerated area. Twelve weeks after injury, no significant nerve regeneration was found in the LC or ET groups, while the sciatic nerve was normal and unimpaired in the SHAM group. Regenerated nerve tissue successfully bridged the 20-mm sciatic nerve defect in the ANG and BCS groups. The yellow arrows represent the positions of the sciatic nerve sutures. (B) Examples of regenerated sciatic nerves from five groups. Tissue specimens show failed nerve regeneration in the LC and ET groups and successful regeneration in the ANG and BCS groups. The regenerated nerves were similar in appearance to those of the SHAM group. The experiments were repeated eight times. (C) The NGF-chitosan scaffold and autologous nerve graft bridged the 20-mm gap, but nerve regeneration in the empty chitosan tube failed. SHAM group: The sciatic nerve was exposed without injury; LC group: 20 mm of the sciatic nerve was removed without treatment; ET group: a 20-mm sciatic nerve gap was bridged with an empty chitosan tube; ANG group: the 20-mm gap in the sciatic nerve was bridged with an autologous nerve graft; BCS group: the BCS was used to bridge the 20-mm gap in the sciatic nerve. ANG: Autologous nerve graft; BCS: biomimetic NGF-chitosan scaffold; ET: empty chitosan tube; LC: lesion control; NGF: nerve growth factor; SHAM: sham-operation.

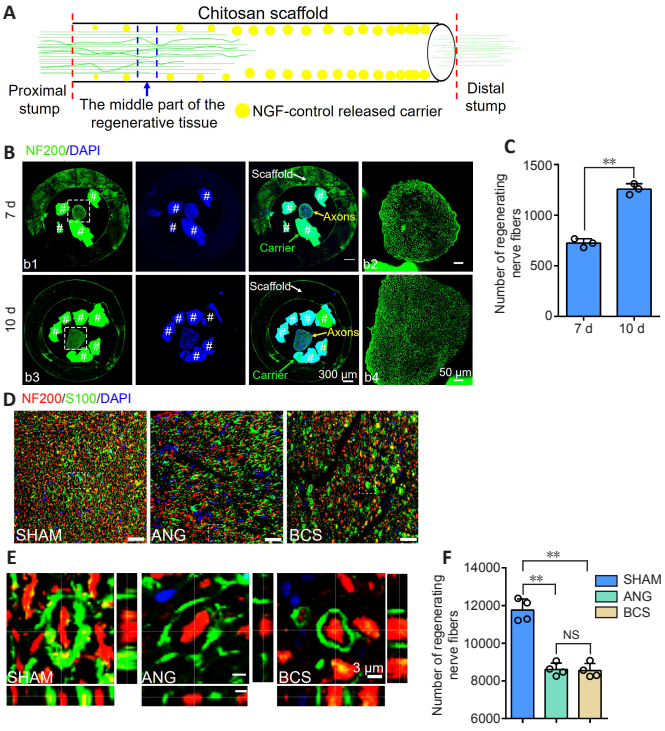

Figure 3 | Sciatic nerve was successfully regenerated after BCS implant.

(A) Schematic diagram of growing axons in the NGF-chitosan scaffold. The chitosan scaffold loaded with the carrier for controlled NGF release promoted the regeneration of the proximal stump of the sciatic nerve. (B) Transverse sections of regenerating nerves 7 or 10 days after bridging the gap in the sciatic nerve with the NGF-chitosan scaffold. Higher magnifications of the boxed areas are also shown. The cross-section of regenerated nerve tissue was larger at 10 days than at 7 days after surgery. #Undegraded NGF controlled-release carrier. Scale bars: 300 μm, 50 μm in enlarged part. (C) Number of regenerated nerve fibers in the middle part of the regenerative tissue between 7 and 10 days after surgery (n = 3 animals per group). $^{**}P$ < 0.01 (Student's t-test). (D) Immunohistochemistry with NF200 (red, Alexa Fluor 594) and S100 (green, Alexa Fluor 488) of the regenerated nerve 12 weeks after surgery. A large number of $NF200^+$ nerve fibers and $S100^+$ myelin sheaths were found in the ANG and BCS groups, but more were seen in the SHAM group. Scale bars: 30 μm. (E) High magnification of the boxed areas in D; Z-stack of confocal images demonstrates co-labeling. Scale bars: 3 μm. (F) At 12 weeks after surgery, the number of $NF200^+$ axons in the middle part of the injured area (n = 4 animals per group). $^{**}P$ < 0.01 (one-way ANOVA followed by Fisher's least significant difference test). Data are presented as mean ± SD. SHAM group: The sciatic nerve was exposed without injury; ANG group: the 20-mm gap in the sciatic nerve was bridged with an autologous nerve graft; BCS group: the BCS was used to bridge the 20-mm gap in the sciatic nerve. ANG: Autologous nerve graft; BCS: biomimetic NGF-chitosan scaffold; DAPI: 4′,6-diamidino-2-phenylindole; ET: empty chitosan tube; LC: lesion control; NF200: neurofilament-200; NGF: nerve growth factor; NS: not significant; SHAM: sham-operation.

BCS facilitates sciatic nerve regeneration

To observe the regenerated sciatic nerve in the BCS (**Figure 3A**), axons were labeled with NF200 antibody at 7 or 10 days after operation. Numerous regenerated axons were thus visible in the transverse sections of regenerated tissue (**Figure 3B**). Statistical analysis showed that the number of regenerated nerve fibers increased significantly between 7 and 10 days after operation in the BCS group (7 days: 1256.7 ± 54.0; 10 days: 723.3 ± 43.0; P < 0.001, n = 3; **Figure 3C**).

Twelve weeks after surgery, longitudinal section analysis showed that the regenerated nerves successfully bridged the 20-mm injured area. In the ANG and BCS groups, $NF200^+$ regenerated nerve fibers were observed in the distal stump of the injured area (**Additional Figure 1**). Numerous axons and myelin sheaths were observed in the transverse sections (**Figure 3D**), and the microscopic structure of the myelin sheath around the axons could be observed in high magnification images (**Figure 3E**). In the BCS group, the chitosan carrier had been completely degraded and a large number of NF200 positive axons were found in the chitosan scaffold (**Additional Figure 2**). There was no significant difference in the number of regenerated axons between the ANG and BCS groups (ANG: 8605.3 ± 340.1; BCSS: 8546.5 ± 383.7; P = 0.859, n = 4; **Figure 3F**), but both were less than the total number of axons in the SHAM group (11729.5 ± 665.9, P < 0.001). In addition, observation of the myelin sheath via toluidine blue staining and transmission electron microscopy showed a large amount of regenerated myelin in the ANG and BCS groups (**Additional Figure 3**).

BCS promotes functional circuit reconstruction

PRV-labeled motoneurons were observed in the L4 spinal cord of the SHAM group, ANG group, and BCS group (**Figure 4A**). We counted the number of PRV-labeled motor neurons, and found no significant difference between the ANG and BCS groups (ANG: 7.3 ± 0.9; BCS: 7.1 ± 1.1; P = 0.776, n = 8, **Figure 4B**). However, the number of PRV-labeled motoneurons was significantly lower in the ANG and BCS groups than in the SHAM group (SHAM: 11.1 ± 1.0, P < 0.001). The sciatic nerve is known to contain many sensory fibers that are directly connected to cell bodies located in the DRG (Dayawansa et al., 2016). We found that many DRG neurons were labeled in the SHAM, ANG and BCS groups (**Figure 4C**). The number of PRV-labeled DRG neurons was significantly lower in the BCS group than in the SHAM group (SHAM: 106.1 ± 7.8; BCS: 63.6 ± 8.4; P < 0.000, n = 8, **Figure 4D**). There was no significant difference between the BCS and ANG groups (BCS: 63.6 ± 8.4; ANG: 64.6 ± 10.2; P = 0.793, n = 8, **Figure 4D**). On this basis, we performed immunofluorescence staining for CGRP positive cells in the DRG. CGRP positive cells are mainly responsible for conducting nociceptive and temperature sensations (McCoy et al., 2013). We found many CGRP positive cells labeled in the DRG (**Figure 4C** and **E**). Many DRG cells were co-labeled with both CGRP and PRV in the ANG and BCS groups (**Figure 4C** and **F**).

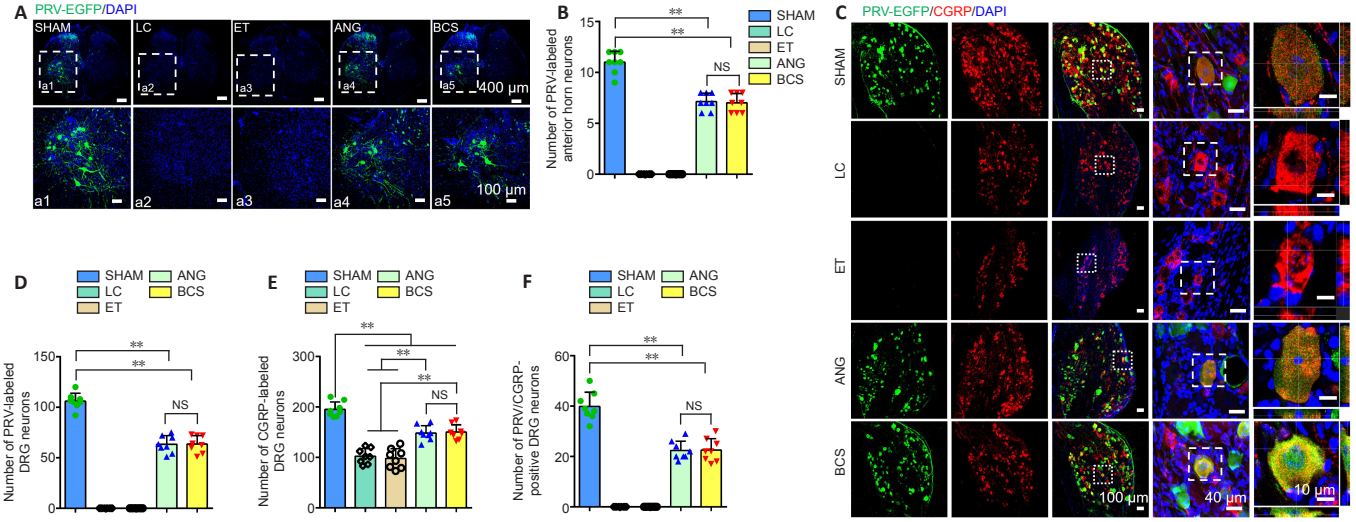

Figure 4 | PRV-labeled motor and sensory neurons 12 weeks after surgery in the rats with sciatic nerve injury repaired with BCS.

(A) PRV mainly labeled motor neurons (green, EGFP) in the ventral horn of the spinal cord. The higher magnifications of the boxed areas shown in A1–5. A large number of PRV-labeled neurons were found in the ANG and BCS groups, but the number was still less than that in the SHAM group. No PRV-labeled neurons were found in the LC or ET groups. Scale bars: 400 μm in the upper row, and 100 μm in the lower row. (B) Number of PRV-labeled anterior horn neurons. (C) PRV-labeled DRG neurons (green, EGFP) and immunofluorescence staining of CGRP (red, Alexa Fluor 594). The higher magnifications of the boxed areas are shown on the right. Z-stack of confocal images demonstrates co-labeling. A large number of neurons co-labeled by PRV and CGRP were found in the ANG and BCS groups, which was less than the number found in the SHAM group. No PRV-labeled neurons were found in the LC or ET groups. Scale bars: 100, 40, and 10 μm, respectively. (D–F) Number of PRV- (D), CGRP- (E) and PRV/CGRP-positive DRG neurons (F). Data are presented as mean ± SD (n = 8 animals per group). $^{**}P < 0.01$ (one-way ANOVA followed by Fisher's least significant difference test). SHAM group: The sciatic nerve was exposed without injury; LC group: 20 mm of the sciatic nerve was removed without treatment; ET group: a 20-mm gap in the sciatic nerve was bridged with an empty chitosan tube; ANG group: the 20-mm gap was bridged with autologous nerve graft; BCS group: the BCS was used to bridge the 20-mm gap in the sciatic nerve. ANG: Autologous nerve graft; BCS: biomimetic NGF-chitosan scaffold; CGRP: calcitonin gene-related peptide; DAPI: 4′,6-diamidino-2-phenylindole; DRG: dorsal root ganglion; EGFP: enhanced green fluorescent protein; ET: empty chitosan tube; LC: lesion control; NGF: nerve growth factor; NS: not significant; PRV: pseudorabies virus; SHAM: sham-operation.

It is worth investigating whether the regenerated sciatic nerve established functional connections with the brain. Brain sections from the SHAM, ANG, and BCS groups showed that PRV-labeled neurons were mainly located in the reticular nucleus (**Figure 5A**), vestibular nucleus (**Figure 5B**), and cerebral cortex (**Figure 5C**). In addition, because of the transsynaptic ability of PRV and the complex connections between brain regions, PRV labeled neurons were also observed in the medial preoptic area, lateral hypothalamus, periaqueductal gray, red nucleus, and locus coeruleus (**Figure 5D** and **E**). However, no PRV labeled neurons were observed in the LC or ET groups. There was no statistically significant difference in the number of PRV-labeled neurons in the reticular nucleus (BCS: 354.6 ± 29.5; ANG: 347.8 ± 35.9; P = 0.779, n = 4), vestibular nucleus (BCS: 67.8 ± 2.2; ANG: 65.5 ± 3.4; P = 0.494, n = 4), and M1 region of motor cortex (BCS: 167.8 ± 18.9; ANG: 172.3 ± 24.0; P = 0.744, n = 4) between the BCS and ANG groups (**Figure 5F–H**). The number of PRV-labeled neurons in all three nuclei was lower in the ANG and BCS groups than in the SHAM group (all $P_s < 0.01$).

BCS enhances sensory and motor functional recovery

The left and right footprints of rats in each group were collected after surgery (**Figure 6A** and **B**). The SFI in the SHAM group remained close to –8.8 for the 12 weeks after surgery (**Figure 6C**), indicating that the motor function in this group was unaffected. From 1 to 12 weeks after operation, the SFI in the LC and ET groups remained around –100. In the ANG group, the SFI began to increase the 4th week after surgery, and continued to increase gradually through the 12th week. In the BCS group, the SFI began to increase the 6th week after surgery, and continued to increase gradually through the 12th week. Twelve weeks after surgery, the SFI did not differ between the ANG and BCS groups (ANG: –52.96 ± 6.29; BCS: –53.34 ± 5.02; P = 0.901, n = 5, **Figure 6C**). This suggests that with the passage of time, motor function in the BCS group gradually recovered to the same levels as are achieved with an autogenous nerve graft.

We used a pinprick assay to evaluate the recovery of sensory function in the plantar skin of each group (**Figure 6D**). The five response areas (from A to E) in the SHAM group responded quickly and forcefully to the pinprick, resulting in a pinprick score of 5 (Sakuma et al., 2016). In the LC and ET groups, the pinprick score was 0 throughout the experimental period. At the 4th week after surgery, one of the five reaction areas of the injured foot in the ANG group began to respond to the pinprick. Over weeks 4 to 12, the number of areas that responded gradually increased. Results were similar in the BCS group, with initial responses in one area beginning at the 5th week after surgery. At the 12th week, all designated areas of the injured foot in the BCS group responded to the pinprick.

BCS relieves muscle atrophy

Twelve weeks after surgery, we removed the left and right tibialis anterior muscles from rats in each group (**Figure 7A**). Atrophy of the muscle on the injured side was severe in the LC and ET groups. Tibialis anterior atrophy also appeared in rats from the ANG and BCS groups, but was less than in the groups that were not treated (**Figure 7C**). The muscle wet weight ratio for the BCS group was significantly worse than that of the SHAM group (BCS: 0.684 ± 0.036; SHAM: 1.005 ± 0.049; P < 0.01, n = 4, **Figure 7C**), but better than those of the LC (0.292 ± 0.025, P < 0.01) and ET groups (0.285 ± 0.061, P < 0.01). There was no significant difference in muscle wet weight ratio between the ANG and BCS groups (BCS: 0.684 ± 0.036; ANG: 0.708 ± 0.068; P = 0.497, n = 4, **Figure 7C**). Next, HE staining was performed on the transverse section of the left tibialis anterior muscle to observe changes in muscle fiber diameter (**Figure 7B**). The diameters of muscle fibers in the SHAM, LC, and ET groups were 84.0 ± 8.98, 11.0 ± 2.58 and 12.0 ± 3.65 μm, respectively. There was no significant difference between the ANG and BCS groups (ANG: 63.5 ± 7.72 μm; BCS: 61.0 ± 7.87 μm; P = 0.604, n = 4, **Figure 7D**). The muscle fiber diameter in both groups was significantly larger than what was observed in the LC or ET groups (P < 0.01), but significantly smaller than that of the SHAM group (P < 0.01). These results indicate that wet muscle weight is maintained, and muscle fiber diameter is larger in the ANG and BCS groups than in untreated rats, thus reducing muscular atrophy.

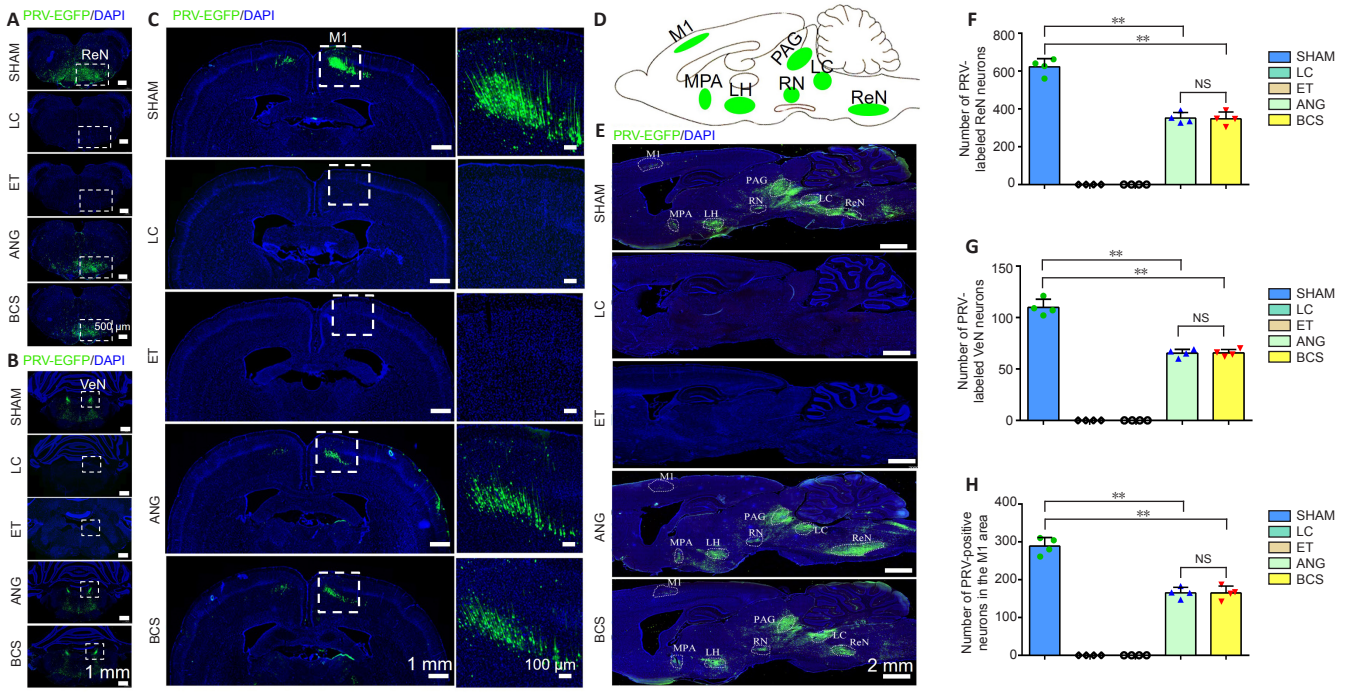

Figure 5 | **PRV-labeled neurons in the brains of rats with sciatic nerve injury repaired via BCS.**
(A–C) PRV-labeled reticular nucleus (ReN, A), vestibular nucleus (VeN, B) and M1 region of the motor cortex (C). A large number of PRV-labeled neurons (green, EGFP) were found in the ReN, VeN, and M1 of SHAM, ANG, and BCS groups, but not in the LC or ET groups. Scale bars: 500 μm in A, 1 mm in B and C, 100 μm in the enlarged part of C. (D) A schematic diagram of PRV-labeled nuclei in brain regions. (E) PRV labeled brain regions (green, EGFP) mainly included primary motor cortex M1 (M1), the medial preoptic area (MPA), lateral hypothalamus (LH), red nucleus (RN), periaqueductal grey (PAG), locus coeruleus (LC), and reticular nucleus (ReN). PRV-labeled neurons were found in multiple brain nuclei in the SHAM, ANG and BCS groups, but not in the LC or ET groups. Scale bars: 2 mm. (F–H) Number of PRV-labeled neurons in the right ReN (F; the boxed areas in A), VeN (G; the boxed areas in B), and M1 region of the motor cortex (H; the boxed areas in C). Data are presented as mean ± SD (n = 4 animals per group). $^{**}P < 0.01$ (one-way analysis of variance followed by Fisher's least significant difference test). SHAM group: The sciatic nerve was exposed without injury; LC group: 20 mm of the sciatic nerve was removed without treatment; ET group: a 20-mm gap in the sciatic nerve was bridged with an empty chitosan tube; ANG group: the 20-mm gap was bridged with autologous nerve graft; BCS group: the BCS was used to bridge the 20-mm gap in the sciatic nerve. ANG: Autologous nerve graft; BCS: biomimetic NGF-chitosan scaffold; CGRP: calcitonin gene-related peptide; DAPI: 4',6-diamidino-2-phenylindole; EGFP: enhanced green fluorescent protein; ET: empty chitosan tube; LC: lesion control; NGF: nerve growth factor; NS: not significant; PRV: pseudorabies virus; SHAM: sham-operation.

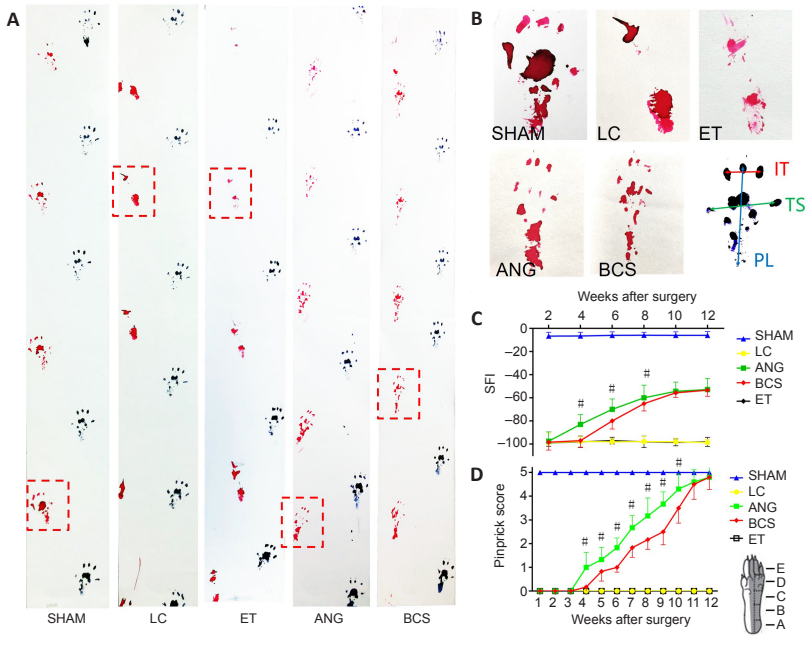

Figure 6 | **Behavioral motor and sensory functional recovery after sciatic nerve injury with BCS repair.**
SHAM group: The sciatic nerve was exposed without injury; LC group: 20 mm of the sciatic nerve was removed without treatment; ET group: a 20-mm gap in the sciatic nerve was bridged with an empty chitosan tube; ANG group: the 20-mm gap was bridged with autologous nerve graft; BCS group: the BCS was used to bridge the 20-mm gap in the sciatic nerve. (A) Rat footprints 12 weeks after surgery. The left footprints were red and the right footprints were blue. Clear and complete red footprints were observed in the SHAM, ANG, and BCS groups, but incomplete footprints were found in the LC and ET groups. (B) Toe imprinting of rats in each group; higher magnifications of the boxed areas in A. Five toes could be observed independently in the SHAM, ANG, and BCS groups, but not in the LC or ET groups. The print length (PL) is the distance from the heel to the third toe, the toe spread (TS) is the distance from the first to fifth toe, and the intermediary toe spread (IT) is the distance between the second and fourth toe. (C) SFI at various times after injury. (D) Pinprick response score after injury (0 = no response and 5 = response in every region of the plantar skin). Data are presented as mean ± SD (n = 5 animals per group). #$P < 0.05$, *vs.* BCS group (Student's t-test). ANG: Autologous nerve graft; BCS: biomimetic NGF-chitosan scaffold; ET: empty chitosan tube; LC: lesion control; NGF: nerve growth factor; SFI: sciatic nerve function index; SHAM: sham-operation.

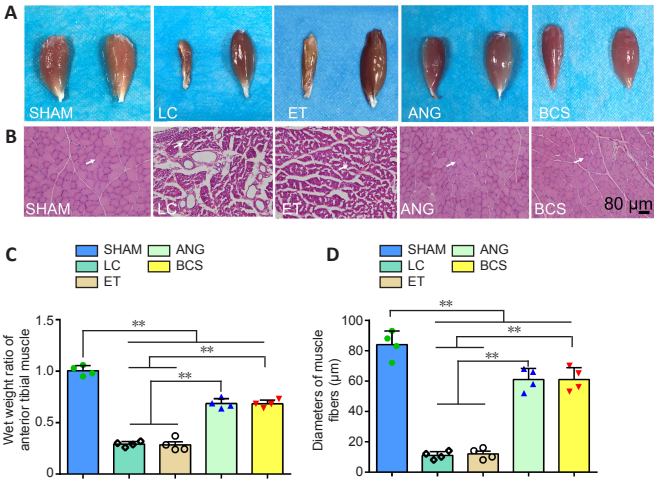

Figure 7 | Atrophy of the anterior tibia muscle 12 weeks after the sciatic nerve injury and BCS repair.

SHAM group: The sciatic nerve was exposed without injury; LC group: 20 mm of the sciatic nerve was removed without treatment; ET group: a 20-mm gap in the sciatic nerve was bridged with an empty chitosan tube; ANG group: the 20-mm gap was bridged with autologous nerve graft; BCS group: the BCS was used to bridge the 20-mm gap in the sciatic nerve. (A) Images of left and right tibialis anterior muscles from rats in each group. Muscular atrophy was absent in the Sham group, severe in the LC and ET groups, and alleviated in the ANG and BCS groups. (B) Hematoxylin-eosin staining of the left tibialis anterior muscle of rats in each group. Correctly patterned muscle fiber arrangement was found in the SHAM, ANG, and BCS groups, while muscle fibers were disordered and the muscle space was enlarged in the LC and ET groups. White arrows indicate muscle fibers in each group. Scale bar: 80 μm. (C) Wet weight ratio of anterior tibialis muscles. (D) Muscle fiber diameter in each group. Data are presented as mean ± SD (n = 4 animals per group). $^{**}P < 0.01$ (one-way analysis of variance followed by Fisher's least significant difference test). ANG: Autologous nerve graft; BCS: biomimetic NGF-chitosan scaffold; ET: empty chitosan tube; LC: lesion control; NGF: nerve growth factor; SHAM: sham-operation.

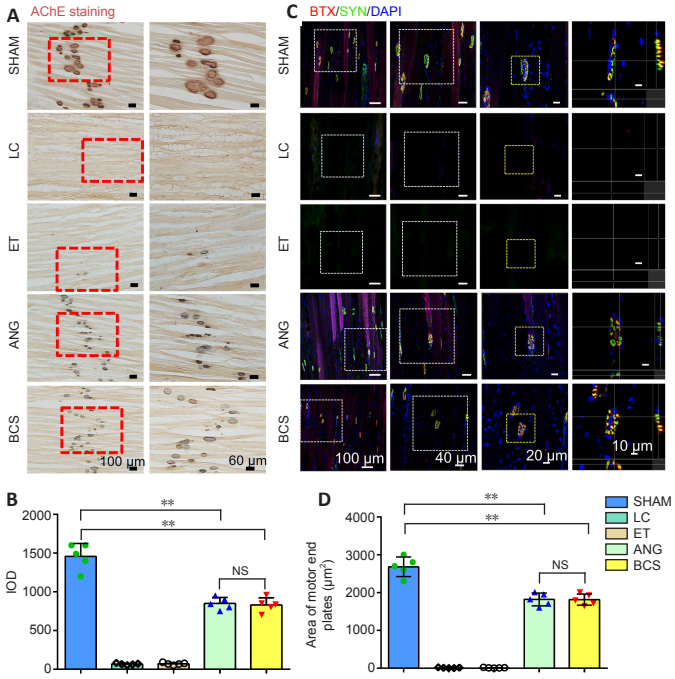

Figure 8 | Reconstruction of motor end plates 12 weeks after sciatic nerve injury and BCS repair.

SHAM group: The sciatic nerve was exposed without injury; LC group: 20 mm of the sciatic nerve was removed without treatment; ET group: a 20-mm gap in the sciatic nerve was bridged with an empty chitosan tube; ANG group: the 20-mm gap was bridged with autologous nerve graft; BCS group: the BCS was used to bridge the 20-mm gap in the sciatic nerve. (A) AChE immunoreactivity (brown) in the motor end plates of the tibialis anterior muscle. Higher magnifications of the boxed areas are shown on the right. AChE was common in SHAM, ANG, and BCS groups, but almost unobservable in LC and ET groups. Scale bars: 100 (left) and 60 (right) μm. (B) Confocal photograph showing immunohistochemical staining with anti-SYN (green, Alexa Fluor 488) and anti-BTX (red, Alexa Fluor 594) in the motor end plates of the tibialis anterior muscle. Higher magnifications of the boxed areas are shown on the right. Z-stack of confocal images demonstrates co-labeling. The presynaptic and postsynaptic membranes of the motor endplate were found in SHAM, ANG, and BCS groups, but no signal was found in the LC or ET groups. Scale bars: 100, 40, 20 and 10 μm, respectively. (C) IOD of AChE staining in each group. (D) Size of motor endplates. Data are presented as mean ± SD (n = 5 animals per group). $^{**}P < 0.01$ (one-way analysis of variance followed by Fisher's least significant difference test). AChE: Acetylcholinesterase; ANG: autologous nerve graft; BCS: biomimetic NGF-chitosan scaffold; BTX: alpha-Bungarotoxin; DAPI: 4′,6-diamidino-2-phenylindole; ET: empty chitosan tube; IOD: integral optical density; LC: lesion control; NGF: nerve growth factor; NS: not significant; SHAM: sham-operation; SYN: synapse1.

BCS increases reinnervation of the motor endplate

Twelve weeks after surgery, stained AChE was brown, smooth edged, and had a clear structure in the SHAM group (**Figure 8A**). In the LC and ET groups, stained AChE was only observed occasionally. In the ANG and BCS groups, stained AChE was numerous, indicating the recovery of AChE activity. There was no significant difference in the IOD of AChE staining between the two groups (ANG: 848.6 ± 79.1; BCS: 829.2 ± 93.7; P = 0.745, n = 5, **Figure 8B**), but it was less for both than for the SHAM group (1457.8 ± 166.7, P < 0.01).

To detect the remodeling of motor endplates in the rats, sections of the left tibialis anterior muscle were stained with SYN and BTX and analyzed for immunofluorescence. In the SHAM group, clear motor endplate structures were observed, including SYN^+ presynaptic membranes and BTX^+ postsynaptic membranes (**Figure 8C**). Similarly, numerous marked motor endplates were observed in the ANG and BCS groups. In contrast, the structures were rarely observed in the presynaptic and post-synaptic membranes of the LC and ET groups, indicating a severe loss of motor function. There was no significant difference in the reconstructed motor endplate areas between the ANG and BCS groups (ANG: 2018.0 ± 347.2 μm^2; BCS: 1812.2 ± 148.6 μm^2; P = 0.128, n = 5, **Figure 8D**), but both areas were smaller than what was seen in the SHAM group (2679.6 ± 258.8 μm^2, P < 0.01). This suggests that regenerated nerves and muscles can help rebuild the motor endplate, thus restoring the contractive function of muscles.

Discussion

Repair of extended peripheral nerve injury remains a great clinical challenge. Current approaches for treatment are promising, but remain insufficient compared with the functional recovery that can be achieved by gold standard autologous nerve transplantation. Although previous work has demonstrated the effectiveness of chitosan scaffolds in improving the quality of nerve regeneration and reducing muscle atrophy in rats (Brown et al., 2015), the studies were either examining short injuries or the degree of peripheral nerve repair was unsatisfactory. The new chitosan scaffold should be able to support axonal growth and nerve regeneration over an extended period of time and over long distances, with the goal of replacing autologous nerve transplantation (Meena et al., 2021). Because the empty nerve conduit lacks the growth factors to induce axons to extend to their targets, the regenerated nerve cannot cross large gaps in injured nerves (Yannas et al., 2007). NGF can promote regenerated axons to grow across the damaged

area and finally extend their growth cones into the target organ to restore motor and sensory function (Makwana and Raivich, 2005). Both chitosan scaffolds and NGF have been studied in a number of experiments, and it is predictable that combining both leads in greater safety in *in vivo* application, avoiding ethical disputes and unnecessary immune reactions. However, the activity of NGF decreases rapidly *in vivo* and cannot support axonal regeneration for extended periods of time (Fang et al., 2020). To solve the above problems, our group developed a new type of controlled release biomaterial, which can slowly release NGF in chitosan scaffolds and provide continuous nutritional support for axonal regeneration. The controlled release technology was based on a controlled release system for neurotrophic factors that was developed in previous studies (Hao et al., 2017; Rao et al., 2018; Oudega et al., 2019). *In vivo*, lysozyme hydrolyzes chitosan to oligosaccharides containing N-acetyl-glucosamine and glucosamine, thus achieving the degradation of chitosan (Pangburn et al., 1982). For the NGF-chitosan scaffold, NGF was able to be released in the chitosan scaffolds for 8 weeks, and the chitosan carrier then began to naturally degrade. The complete degradation of the chitosan scaffold took at least two years in rats.

In this study, the chitosan scaffold not only provided a traditional regeneration environment, but also improved the elasticity of the chitosan scaffold, which helped it avoid compressing and damaging the surrounding tissue. General observation and immunofluorescence staining of the regenerated nerve showed that the large gap (20 mm) in the BCS group was bridged successfully. In most studies of using scaffolds to repair peripheral nerve injury, the tracers that were used did not cross the synapse, such as fluorogold, DiI, cholera toxin B subunit, and hydrogen peroxidase (Han et al., 2015; Bozkurt et al., 2016; Zhang et al., 2020). In our study, we used a retrograde tracer which was helpful for clearly observing whether the regenerated nerve has successfully reconnected with the central nervous system. The PRV results showed that the regenerated sciatic nerves in the ANG and BCS groups reconnected with anterior horn motoneurons and sensory neurons in the DRG, and established formed synapses with neurons in the central nervous system. Xing et al. (2020) previously found that whole brain activity was significantly reduced in a rat model of sciatic nerve injury, and alterations in connectivity between resting-state networks verified the damage in motor-related functional neural circuits. In contrast, the regenerated sciatic nerves in the current study successfully established functional neural circuits similar to those of normal sciatic nerves. Combined with the results of the behavioral analysis, our results indicated that the function of the damaged nerves was partially restored in the ANG and BCS groups. We speculate that the decrease in brain activity observed in Xing et al. (2020) was mainly due to a decrease in the number of connections between the brain and neurons in the injured nerve. In that case, sensory and motor functions of the damaged nerve could not fully recover after peripheral nerve injury.

The pinprick assay showed that the rats receiving the BCS transplant had a response to mechanically induced nociceptive sensation 5 weeks after surgery. At this time, it can be speculated that the regenerated nerve has crossed the large gap in the injured area and re-connected with nociceptors in the skin. The SFI results showed that motor function in the BCS group began to recover by the 6th week. This suggests that the regenerated sciatic nerve crossed the injured area and re-innervated the muscles. It is worth noting that sensory function in rats recovered earlier than motor function, which is likely because the structure of sensory nerve endings is relatively simpler than that of motor endplates. Additionally, unlike motor fibers, nociceptor sensory fibers are not myelinated. It is possible that sensory and motor fibers regenerate at similar rates, but that subsequent myelination leads to the recovery-time differences that we observed. As a result, sensory functions can be recovered earlier and more easily, which is consistent with the results of Ma et al. (2011).

The motor endplate structure includes the presynaptic membrane, synaptic space, and postsynaptic membrane (Rudolf et al., 2019). Acetylcholine is released from the presynaptic membrane into the synaptic space and reaches the postsynaptic membrane to bind to its receptor, then it is quickly hydrolyzed by AChE to prevent continuous muscle excitation (Güller et al., 2020). If the motor endplate structure of the muscle is destroyed because of denervation and no release of acetylcholine, AChE will gradually be metabolized and disappear (Zhou et al., 2020). Therefore, we used AChE staining and immunofluorescence staining to assess the functional recovery of the motor endplate. What cannot be ignored is that animals that have physical impairments are likely to experience atrophy on the non-experimental side as well as the experimental side because of a reduced amount of overall movement. This can potentially bias the measurements and lead to a higher wet-weight ratio of muscles. The effect of unilateral sciatic nerve injury on contralateral muscle atrophy needs to be verified by further experiments.

Although the BCS transplant was able to repair extensive sciatic nerve injury in rats, the clinical application of the BCS needs to be verified in experiments using larger animals, such as sheep or rhesus monkeys. In addition, although a large number of studies have been conducted on the molecular mechanism through which NGF promotes nerve regeneration, this study focused only on the outcomes of animal experiments, but did not verify the molecular mechanisms involved in BCS-related recovery. To further improve the outcomes of chitosan scaffolds in repairing peripheral nerve injury, future BCS-based chitosan scaffolds can combine multiple neurotrophic factors.

In conclusion, chitosan scaffolds have been studied extensively in previous experiments. However, for treating peripheral nerve injury in rats, the previous chitosan scaffolds loaded with NGF either failed to reach the level of repair that can be achieved via ANG, or the length of the nerve damage was short (< 20 mm). At the same time, the duration of NGF release in chitosan scaffolds was relatively short (< 40 days), which may not be suitable for treating long (20 mm) sciatic nerve defect in rats. The current study was the first test using a chitosan scaffold containing control-released (8 weeks) NGF for repairing 20-mm gaps in the sciatic nerve of Wistar rats. The SFI and pinprick-assay score gradually improved after BCS transplant. By 12 weeks after injury, a large number of regenerated $NF200^+$ axons and $S100^+$ myelin sheaths were observed. The regenerated sciatic nerve successfully established a functional neural connection with the reticular nucleus, vestibular nucleus, red nucleus, and motor cortex. Muscle wet weight ratio was maintained, and muscular atrophy was improved. SYN^+ presynaptic membranes and BTX^+ postsynaptic membranes were observed in immunofluorescent stained sections, indicating the reconstruction of neuromuscular junctions between the regenerated nerve and muscle. Therefore, implanting a BCS led to a level of repair that was equivalent to what can be achieved with autologous nerve transplantation. Thus, BCS represents a potential new treatment option for patients with peripheral nerve injury, which has a prospect for broad clinical application.

Author contributions: *Study conception, design and definition of intellectual content: FDL, PH, ZYY, XGL; literature search and experimental studies: FDL, HMD; data acquisition and analysis: FDL, HMD, FH, WZ, YDG; manuscript preparation, editing and review: FDL, PH, ZYY, XGL. All authors read and approved the final manuscript.*
Conflicts of interest: *The authors declare that they have no conflicts of interest.*

Financial support: *This study was supported by the National Natural Science Foundation of China, Nos. 31900749 (to PH), 31730030 (to XGL), 81941011 (to XGL), 31971279 (to ZYY), 31771053 (to HMD); and the Natural Science Foundation of Beijing of China, No. 7214301 (to FH). The funding sources had no role in study conception and design, data analysis or interpretation, paper writing or deciding to submit this paper for publication.*
Institutional review board statement: *This study was approved by the Animal Ethics Committee of Capital Medical University (approval No. AEEI-2017-033) on March 21, 2017.*

Data sharing statement: *Datasets analyzed during the current study are available from the corresponding author on reasonable request.*
Plagiarism check: *Checked twice by iThenticate.*
Peer review: *Externally peer reviewed.*

Open peer reviewers: *Artur S.P. Varejão, University of Trás-os-Montes e Alto Douro, Portugal; Zhengchao Guo, Universiteit Twente, Netherlands.*
Additional files:
Additional Figure 1: *The sciatic nerve was successfully regenerated at 12 weeks after sciatic nerve injury.*
Additional Figure 2: *Image of successful regeneration of injured sciatic nerve in the biomimetic nerve growth factor-chitosan scaffold (BCS).*
Additional Figure 3: *Morphological analysis of regenerated myelin sheaths at 12 weeks after sciatic nerve injury.*
Additional file 1: *Open peer review reports 1 and 2.*

References

Bain JR, Mackinnon SE, Hunter DA (1989) Functional evaluation of complete sciatic, peroneal, and posterior tibial nerve lesions in the rat. Plast Reconstr Surg 83:129-138.
Bozkurt A, Boecker A, Tank J, Altinova H, Deumens R, Dabhi C, Tolba R, Weis J, Brook GA, Pallua N, van Neerven SGA (2016) Efficient bridging of 20 mm rat sciatic nerve lesions with a longitudinally micro-structured collagen scaffold. Biomaterials 75:112-122.
Brown AD, Jones HG, Kan A, Thakkar T, Stecker GC, Goupell MJ, Litovsky RY (2015) Evidence for a neural source of the precedence effect in sound localization. J Neurophysiol 114:2991-3001.
Cao ZR, Zheng B, Zhong L, Hu LC, Zhang XL, Qu B, Jiang T (2019)Collagen/heparin sulfate scaffold combined with neural stem cells promote motor function recovery after spinal cord injury. Zhongguo Zuzhi Gongcheng Yanjiu 23:5454-5461.
Das KK, Srivastava AK (2019) Nerve conduits as replacements of autografts in peripheral nerve surgery: Still a work in progress. Neurol India 67:S115-s117.
Dayawansa S, Zhang J, Shih CH, Tharakan B, Huang JH (2016) Functional, electrophysiological recoveries of rats with sciatic nerve lesions following transplantation of elongated DRG cells. Neurol Res 38:352-357.
Fang Z, Ge X, Chen X, Xu Y, Yuan WE, Ouyang Y (2020) Enhancement of sciatic nerve regeneration with dual delivery of vascular endothelial growth factor and nerve growth factor genes. J Nanobiotechnology 18:46.
Fu CY, Zhao J, Qu W (2013) Tissue-engineered nerve for repair of peripheral nerve injuries. Zhongguo Zuzhi Gongcheng Yanjiu 17:7335-7340.
Gu X, Ding F, Yang Y, Liu J (2011) Construction of tissue engineered nerve grafts and their application in peripheral nerve regeneration. Prog Neurobiol 93:204-230.
Güller U, Güller P, Çiftci M (2020) Radical scavenging and antiacetylcholinesterase activities of ethanolic extracts of carob, clove, and linden. Altern Ther Health Med.
Han Q, Cao C, Ding Y, So KF, Wu W, Qu Y, Zhou L (2015) Plasticity of motor network and function in the absence of corticospinal projection. Exp Neurol 267:194-208.
Hao P, Duan H, Hao F, Chen L, Sun M, Fan KS, Sun YE, Williams D, Yang Z, Li X (2017) Neural repair by NT3-chitosan via enhancement of endogenous neurogenesis after adult focal aspiration brain injury. Biomaterials 140:88-102.
Jia F, Lv P, Miao H, Shi X, Mei H, Li L, Xu X, Tao S, Xu F (2019) Optimization of the fluorescent protein expression level based on pseudorabies virus bartha strain for neural circuit tracing. Front Neuroanat 13:63.
Kemp SW, Webb AA, Dhaliwal S, Syed S, Walsh SK, Midha R (2011) Dose and duration of nerve growth factor (NGF) administration determine the extent of behavioral recovery following peripheral nerve injury in the rat. Exp Neurol 229:460-470.
Kornfeld T, Nessler J, Helmer C, Hannemann R, Waldmann KH, Peck CT, Hoffmann P, Brandes G, Vogt PM, Radtke C (2021) Spider silk nerve graft promotes axonal regeneration on long distance nerve defect in a sheep model. Biomaterials 271:120692.
Lackington WA, Kočí Z, Alekseeva T, Hibbitts AJ, Kneafsey SL, Chen G, O'Brien FJ (2019) Controlling the dose-dependent, synergistic and temporal effects of NGF and GDNF by encapsulation in PLGA microparticles for use in nerve guidance conduits for the repair of large peripheral nerve defects. J Control Release 304:51-64.
Li R, Li Y, Wu Y, Zhao Y, Chen H, Yuan Y, Xu K, Zhang H, Lu Y, Wang J, Li X, Jia X, Xiao J (2018) Heparin-poloxamer thermosensitive hydrogel loaded with bFGF and NGF enhances peripheral nerve regeneration in diabetic rats. Biomaterials 168:24-37.
Liu F, Hao F, Hao P, Zhao W, Gao Y, Duan H, Yang Z, Li X (2021) bFGF-chitosan scaffolds effectively repair 20 mm sciatic nerve defects in adult rats. Biomed Mater 16:025011.
Ma CH, Omura T, Cobos EJ, Latremoliere A, Ghasemlou N, Brenner GJ, van Veen E, Barrett L, Sawada T, Gao F, Coppola G, Gertler F, Costigan M, Geschwind D, Woolf CJ (2011) Accelerating axonal growth promotes motor recovery after peripheral nerve injury in mice. J Clin Invest 121:4332-4347.
Makwana M, Raivich G (2005) Molecular mechanisms in successful peripheral regeneration. FEBS J 272:2628-2638.
Marquardt LM, Sakiyama-Elbert SE (2013) Engineering peripheral nerve repair. Curr Opin Biotechnol 24:887-892.
McCoy ES, Taylor-Blake B, Street SE, Pribisko AL, Zheng J, Zylka MJ (2013) Peptidergic CGRPα primary sensory neurons encode heat and itch and tonically suppress sensitivity to cold. Neuron 78:138-151.
Meena P, Kakkar A, Kumar M, Khatri N, Nagar RK, Singh A, Malhotra P, Shukla M, Saraswat SK, Srivastava S, Datt R, Pandey S (2021) Advances and clinical challenges for translating nerve conduit technology from bench to bed side for peripheral nerve repair. Cell Tissue Res 383:617-644.
Mohamadi F, Ebrahimi-Barough S, Nourani MR, Ahmadi A, Ai J (2018) Use new poly (ε-caprolactone/collagen/NBG) nerve conduits along with NGF for promoting peripheral (sciatic) nerve regeneration in a rat. Artif Cells Nanomed Biotechnol 46:34-45.
Navarro X, Vivó M, Valero-Cabré A (2007) Neural plasticity after peripheral nerve injury and regeneration. Prog Neurobiol 82:163-201.
Oudega M, Hao P, Shang J, Haggerty AE, Wang Z, Sun J, Liebl DJ, Shi Y, Cheng L, Duan H, Sun YE, Li X, Lemmon VP (2019) Validation study of neurotrophin-3-releasing chitosan facilitation of neural tissue generation in the severely injured adult rat spinal cord. Exp Neurol 312:51-62.
Pangburn SH, Trescony PV, Heller J (1982) Lysozyme degradation of partially deacetylated chitin, its films and hydrogels. Biomaterials 3:105-108.
Rao F, Wang Y, Zhang D, Lu C, Cao Z, Sui J, Wu M, Zhang Y, Pi W, Wang B, Kou Y, Wang X, Zhang P, Jiang B (2020) Aligned chitosan nanofiber hydrogel grafted with peptides mimicking bioactive brain-derived neurotrophic factor and vascular endothelial growth factor repair long-distance sciatic nerve defects in rats. Theranostics 10:1590-1603.
Rao JS, Zhao C, Zhang A, Duan H, Hao P, Wei RH, Shang J, Zhao W, Liu Z, Yu J, Fan KS, Tian Z, He Q, Song W, Yang Z, Sun YE, Li X (2018) NT3-chitosan enables de novo regeneration and functional recovery in monkeys after spinal cord injury. Proc Natl Acad Sci U S A 115:E5595-E5604.
Rudolf R, Khan MM, Witzemann V (2019) Motor endplate-anatomical, functional, and molecular concepts in the historical perspective. Cells 8:387.
Sakuma M, Gorski G, Sheu SH, Lee S, Barrett LB, Singh B, Omura T, Latremoliere A, Woolf CJ (2016) Lack of motor recovery after prolonged denervation of the neuromuscular junction is not due to regenerative failure. Eur J Neurosci 43:451-462.
Wang H, Zhao Q, Zhao W, Liu Q, Gu X, Yang Y (2012) Repairing rat sciatic nerve injury by a nerve-growth-factor-loaded, chitosan-based nerve conduit. Biotechnol Appl Biochem 59:388-394.
Wang Y, Wang S, He JH (2021) Transcriptomic analysis reveals essential microRNAs after peripheral nerve injury. Neural Regen Res 16(9):1865-1870.
Xia B, Lv Y (2018) Dual-delivery of VEGF and NGF by emulsion electrospun nanofibrous scaffold for peripheral nerve regeneration. Mater Sci Eng C Mater Biol Appl 82:253-264.
Xing XX, Hua XY, Zheng MX, Ma ZZ, Huo BB, Wu JJ, Ma SJ, Ma J, Xu JG (2020) Intra and inter: alterations in functional brain resting-state networks after peripheral nerve injury. Brain Behav 10:e01747.
Xu H, Yan Y, Li S (2011) PDLLA/chondroitin sulfate/chitosan/NGF conduits for peripheral nerve regeneration. Biomaterials 32:4506-4516.
Yang Z, Zhang A, Duan H, Zhang S, Hao P, Ye K, Sun YE, Li X (2015) NT3-chitosan elicits robust endogenous neurogenesis to enable functional recovery after spinal cord injury. Proc Natl Acad Sci U S A 112:13354-13359.
Yannas IV, Zhang M, Spilker MH (2007) Standardized criterion to analyze and directly compare various materials and models for peripheral nerve regeneration. J Biomater Sci Polym Ed 18:943-966.
Yi S, Xu L, Gu X (2019) Scaffolds for peripheral nerve repair and reconstruction. Exp Neurol 319:112761.
Zhang RC, Du WQ, Zhang JY, Yu SX, Lu FZ, Ding HM, Cheng YB, Ren C, Geng DQ (2021) Mesenchymal stem cell treatment for peripheral nerve injury: a narrative review. Neural Regen Res 16(11):2170-2176.
Zhang Y, Zhang Y, Tian K, Wang Y, Fan X, Pan Q, Qin G, Zhang D, Chen L, Zhou J (2020) Calcitonin gene-related peptide facilitates sensitization of the vestibular nucleus in a rat model of chronic migraine. J Headache Pain 21:72.
Zhou L, Huang YF, Xie H, Mei XY, Cao J (2020) Herbal complex 'Buyang Huanwu Tang' improves motor endplate function of denervated-dependent skeletal muscle atrophy in rat. J Integr Neurosci 19:89-99.

P-Reviewers: Varejão ASP, Guo Z; C-Editor: Zhao M; S-Editors: Yu J, Li CH; L-Editors: Yu J, Song LP; T-Editor: Jia Y

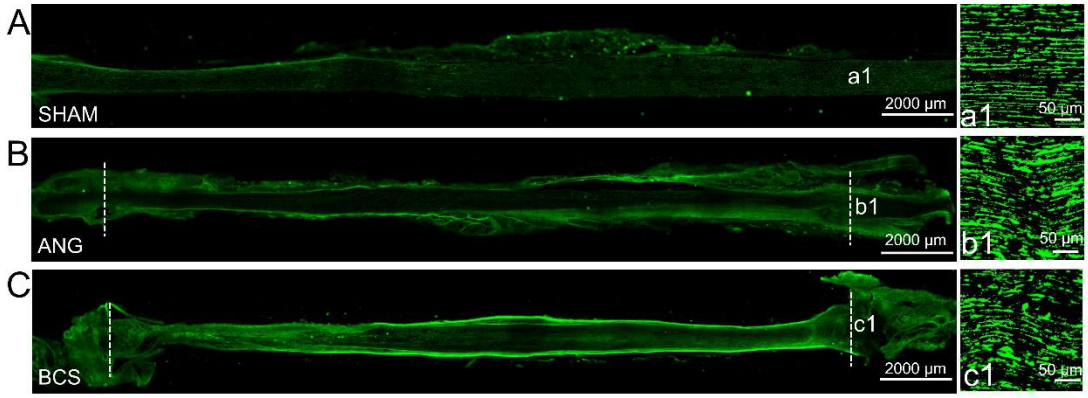

Additional Figure 1 The sciatic nerve was successfully regenerated at 12 weeks after sciatic nerve injury.

SHAM group: The sciatic nerve was exposed without injury; ANG group: the 20 mm sciatic nerve gap was bridged with autologous nerve graft; BCS group: the BCS was used to bridge the 20 mm sciatic nerve gap. (A-C) Immunohistochemistry with anti-NF200 (green, Alexa Fluor 488) of the sciatic nerve in the SHAM group (A), ANG group (B), BCS group (C). The nerve fibers were orderly arranged in the SHAM group, but disorderly arranged in the ANG and BCS groups. The dotted lines mean suture sites. The position of a1, b1 and c1 represented the distal stump of the nerve. Also shown were the higher magnification images, respectively. Scale bars: 2000 μm in A-C, 50 μm in a1-c1. The experiments were repeated by four times (*n* = 4 animals per group). ANG: Autologous nerve graft; BCS: biomimetic nerve growth factor-chitosan scaffold; NF200: neurofilament proteins 200; SHAM: sham-operation.

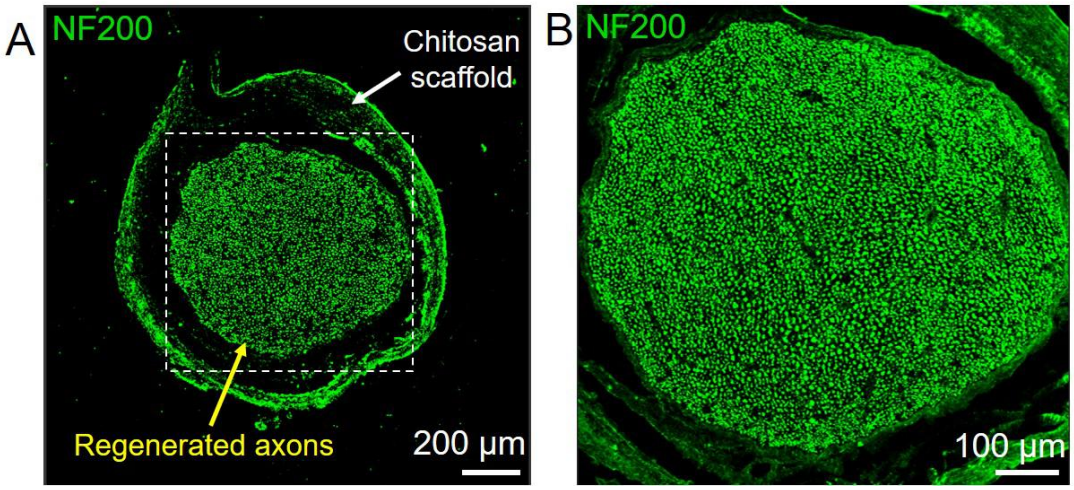

Additional Figure 2 Image of successful regeneration of injured sciatic nerve in the biomimetic nerve growth factor-chitosan scaffold (BCS).

(A) Immunohistochemistry with anti-NF200 (green, Alexa Fluor 488) of the sciatic nerve in the BCS group. The section was from the middle position of the scaffold. At 12 weeks postoperatively, no chitosan carrier was observed and degradation of the chitosan scaffold was observed. The yellow arrow indicated regenerated axons and the white arrow indicated chitosan scaffold. (B) High magnification of the boxed areas in A. Scale bars: 200 μm in A, 100 μm in B. The experiments were repeated by four times (*n* = 4 animals). NF200: Neurofilament proteins 200.

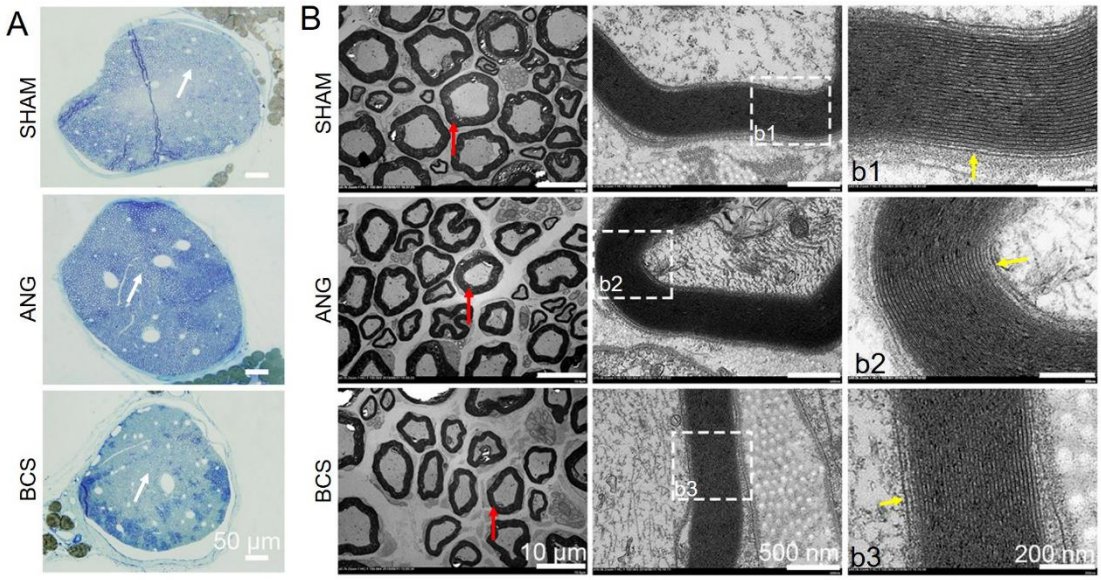

Additional Figure 3 Morphological analysis of regenerated myelin sheaths at 12 weeks after sciatic nerve injury.

SHAM group: The sciatic nerve was exposed without injury; ANG group: the 20 mm sciatic nerve gap was bridged with autologous nerve graft; BCS group: the BCS was used to bridge the 20 mm sciatic nerve gap. The sections were taken from the central site of the injury area (*n* = 4 animals per group). (A) Toluidine blue stained myelin sheaths. Large amounts of myelin were stained with toluidine blue in the ANG and BCS groups, as well as in the SHAM group. The white arrow indicated the myelin sheath. The semi-thin sections were incubated with 1% toluidine blue dye for 10 minutes at room temperature, and observed under a microscope (BX-51, Olympus, Tokyo, Japan). (B) Transmission electron micrographs showing the ultrastructure of myelin sheaths. The higher magnification images of box areas in the middle column were shown in b1-3. The red arrow indicated the myelin sheath, the yellow arrow indicated the myelin lamina. The ultra-thin sections of 60 nm thicknesses were observed under a transmission electron microscope (HT7700, Hitachi, Tokyo, Japan). The higher magnifications of the boxed areas were shown in right images. The experiments were repeated by four times (*n* = 4 animals per group). Scale bars: 50 μm in A, 10 μm, 500 nm, 200 nm in B. ANG: Autologous nerve graft; BCS: biomimetic nerve growth factor-chitosan scaffold; SHAM: sham-operation.